Phase Stability and Transition of $BaSi_2$-type Disilicides and Digermanides

Jian-Tao Wang,[1,2,*] Changfeng Chen,[2] and Yoshiyuki Kawazoe[3,4]

[1]*Beijing National Laboratory for Condensed Matter Physics, Institute of Physics, Chinese Academy of Sciences, Beijing 100190, China*
[2]*Department of Physics and High Pressure Science and Engineering Center, University of Nevada, Las Vegas, Nevada 89154, USA*
[3]*New Industry Creation Hatchery Center, Tohoku University, Sendai 980-8579, Japan*
[4]*Institute of Thermophysics, Siberian Branch of Russian Academy of Sciences, Novosibirsk 630090, Russia*

(Dated: October 18, 2014)

$BaSi_2$-type disilicides and digermanides hold great promise for solar-cell applications, but their structural stability and phase transition mechanisms remain unresolved. Here we present *ab initio* calculations of pressure induced structural phase transitions of $BaSi_2$, $BaGe_2$ and $SrGe_2$ and show that Si-tetrahedra in orthorhombic $BaSi_2$ tend to convert to corrugated layers in the trigonal phase under high pressure with bond breaking along the b-axis, and a three-dimensional Si-net in the cubic phase is stabilized energetically at low pressure. The orthorhombic-to-trigonal conversion is also preferred for $SrGe_2$ by both energetics and kinetics. However, Ge-tetrahedra in $BaGe_2$ tends to convert to a $ThSi_2$-type tetragonal net with bond breaking around the c-axis. The kinetic barriers are large for both the reaction ($\sim$0.43 eV under compression) and counterreaction ($\sim$0.39 eV under decompression) for $BaSi_2$, which explains the stability of the trigonal and cubic phases at room temperature and the high-temperature requirement for the phase transitions.

$BaSi_2$-type disilicides and digermanides $BaSi_2$, $SrSi_2$, $BaGe_2$, and $SrGe_2$ are semiconductors with larger energy gaps of 0.9$\sim$1.3 eV and high optical absorption coefficients [1–5], which make them ideal candidates as silicon-based solar cell materials. Great interest in these materials has been reignited by recent success in preparing well-crystalline a-axis-oriented $BaSi_2$ and $Ba_{1-x}Sr_xSi_2$ epitaxial films on Si(111) and Si(100) substrates [6–11]. It was demonstrated that the electronic band gap can reach the ideal value of approximately 1.4 eV by replacing half of the Ba atoms with isoelectric Sr atoms [6]. At ambient conditions, $BaSi_2$, $BaGe_2$, and $SrGe_2$ all adopt the $BaSi_2$-type orthorhombic structure, but $SrSi_2$ has the $SrSi_2$-type cubic structure [12–18]. Under high-pressure and high-temperature (HTHP) conditions, orthorhombic $BaSi_2$ transforms into $SrSi_2$-type cubic and $EuGe_2$-type trigonal structure [19, 20], and cubic $SrSi_2$ transforms into α-$ThSi_2$-type tetragonal structure [21]. On the other hand, orthorhombic $BaGe_2$ and $SrGe_2$ [22–24] transform into tetragonal and trigonal structure, respectively. Each phase of disilicides and digermanides is characterized by a unique Si or Ge configuration: isolated tetrahedra in the orthorhombic phase, two-dimensional three-connected (2D3C) corrugated layers in the trigonal phase, and three-dimensional three-connected (3D3C) nets in both cubic and tetragonal phases. Past studies have explored the electronic, thermoelectric and optical properties of these materials [25–27], but the more complicated and important atomistic mechanisms for the phase stability and pressure induced phase transformations remain unresolved.

In this Letter, we present a comprehensive study on the phase stability and transition of $BaSi_2$ compared with $BaGe_2$ and $SrGe_2$ under a wide pressure range of $0 \sim 10$ GPa. We examine the energetics and kinetics that govern the phase stability and drive the structural conversion. In particular, we identify the pathways from the tetrahedra configurations in the orthorhombic phase toward the 2D3C corrugated layers in the trigonal phase and the 3D3C nets in the cubic phase with the Si-Si bond breaking and reconstruction parallel to the b[010] axis. The Si-tetrahedra in orthorhombic $BaSi_2$ convert to corrugated layers dynamically under high pressure, which further convert to 3D3C cubic net under low pressure (< 7 GPa) driven by energetics. Direct conversion from the orthorhombic to trigonal structure is also favored for $SrGe_2$ by both energetics and kinetics. Moreover, Ge-tetrahedra in $BaGe_2$ tend to form 3D3C tetragonal net structure with bond breaking and rebonding around the c[001] axis. Pressure plays a key role in enhancing the HP production stability, but it has little effect on the conversion barrier. The large counterreaction barriers ($\sim$0.39 eV) are comparable to the compression process reaction barriers ($\sim$0.43 eV) for $BaSi_2$, which explains the high stability of the HPHT metastable phases at room temperature and the requirement of high temperature for the phase transitions [20], in contrast to low-kinetic-barrier cold-compressed phase transitions in Si and Ge [28].

Our calculations are carried out using density functional theory as implemented in the Vienna *ab initio* simulation package (VASP) [29] with the spin-polarized generalized gradient approximation (GGA) [30]. The all-electron projector augmented wave (PAW) method [31] was adopted with $4s^24p^65s^2$ for Sr, $5s^25p^66s^2$ for Ba, $3s^23p^2$ for Si, and $3d^{10}4s^24p^2$ for Ge treated as valence electrons. A plane-wave basis set with an energy cutoff of 500 eV was used. The phase conversion barrier was calculated using a generalized solid-state nudged elastic band method [32] with the cell and atomic position optimization. Forces on the ions are calculated through the

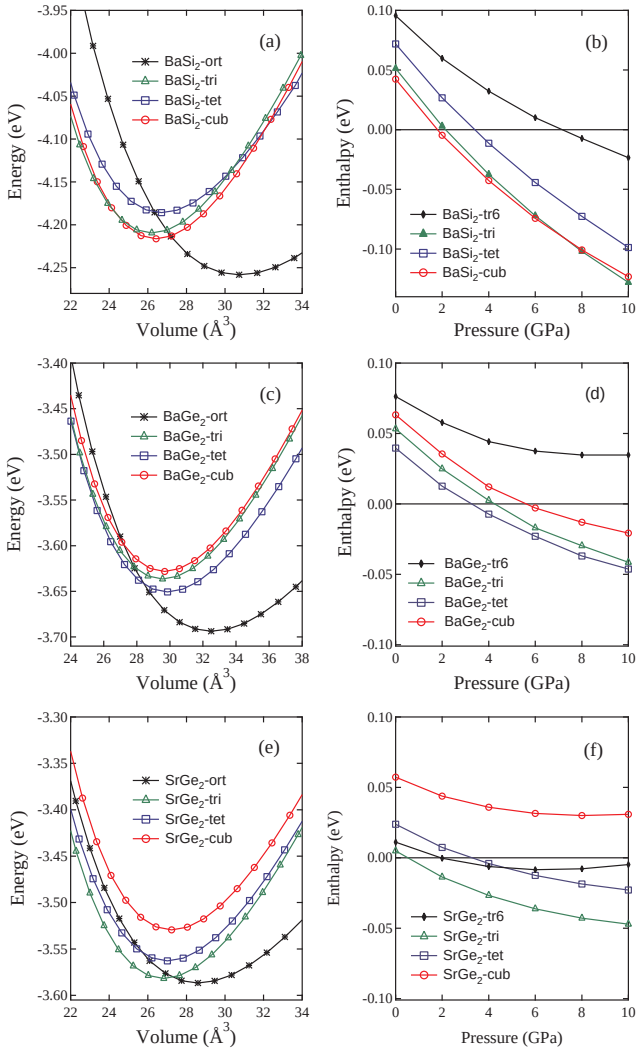

FIG. 1: (color online) Energy versus volume per atom for $BaSi_2$ (a), $BaGe_2$ (c), and $SrGe_2$ (e). Enthalpy per atom versus pressure for $BaSi_2$ (b), $BaGe_2$ (d), and $SrGe_2$ (f), relative to that of $BaSi_2$-type orthorhombic structure. The $BaSi_2$-type orthorhombic (*ort*), $SrSi_2$-type cubic (*cub*), α-$ThSi_2$ type tetragonal (*tet*) and $EuGe_2$-type trigonal (*tri*) phases are in D_{2h}^{16}-*Pnma*, O^6-$P4_332$, D_{4h}^{19}-$I4_1/amd$, and D_{3d}^3-$P\bar{3}m1$ symmetry, respectively. The enthalpy of $CaSi_2$-type structure (*tr*6 in $R\bar{3}m$ symmetry) [33] is shown for comparison.

Hellmann-Feynman theorem allowing a full geometry optimization. Convergence criteria employed for both the electronic and the ionic relaxation were set to 10^{-6} eV and 0.02 eV/Å for energy and force, respectively.

We first discuss the energetic stability of silicides and germanides. The results (Fig. 1) show that the most favorable structures are orthorhombic with relatively large volumes of 30.78, 32.53, and 28.61 Å^3 per atom for $BaSi_2$, $BaGe_2$, and $SrGe_2$, respectively. Meanwhile, the second stable phases have distinct cubic, tetragonal, and trigonal structures with a relatively small volume of 26.43, 29.86, and 26.83 Å^3 per atom. Upon compression, for $BaSi_2$ as shown in Fig. 2(b), the cubic structure becomes more stable than the orthorhombic structure at 1.9 GPa, and the trigonal structure becomes more stable than the cubic structure above 7.2 GPa. The larger enthalpy change between the orthorhombic and cubic phases shows a strong pressure dependence with a large volume change, while the small enthalpy change between the cubic and trigonal phases has a corresponding small volume change (see Table I). On the other hand, for $BaGe_2$ and $SrGe_2$ as shown in Fig. 1(d,f), no stable cubic phase exists up to 10 GPa. The tetragonal and trigonal structure become more stable than the orthorhombic structure above 3.2 GPa and 0.52 GPa, respectively, showing a strong size-selecting rule to find best matching between the Ge or Si sublattice and metal atoms. The enthalpy of the $CaSi_2$-type structure (*tr*6 in $R\bar{3}m$ symmetry) is also shown in Fig. 2(b,d,f) for comparison [33], but it is clearly unfavorable for $BaSi_2$, $BaGe_2$, and $SrGe_2$ under a wide pressure range of $0 \sim 10$ GPa.

We next examine the kinetic process at the atomic scale using a generalized solid-state climbing image nudged elastic band method [32] with the cell and atomic positions optimization under a wide pressure range of 0∼8 GPa. According to above results, there are three possible phase transformations from $BaSi_2$-type orthorhombic structure toward the $SrSi_2$-type cubic,

TABLE I: Calculated equilibrium lattice parameters a, b, c (in Å),volume (in Å^3 per atom), and bulk modulus (B_0 in GPa) for $BaSi_2$, $BaGe_2$ and $SrGe_2$ in orthorhombic (ort), cubic (cub), tetragonal (tet), and trigonal (tri) symmetry at 0 GPa, compared to available experimental data [17, 18, 20, 22, 23, 33].

Phase	Method	a (Å)	b (Å)	c (Å)	V_0 (Å^3)	B_0 (GPa)
$BaSi_2$-ort	Cal	9.224	6.827	11.716	30.78	28.23
	Exp [20]	8.942	6.733	11.555	28.99	27.94
$BaSi_2$-tri	Cal	4.102	4.102	5.445	26.41	44.46
	Exp [20]	4.047	4.047	5.330	25.21	
$BaSi_2$-cub	Cal	6.820	6.820	6.820	26.43	48.24
	Exp [20]	6.715	6.715	6.715	25.24	
$BaSi_2$-tet	Cal	4.736	4.736	14.287	26.71	40.84
$BaGe_2$-ort	Cal	9.471	6.942	11.861	32.53	25.14
	Exp [22]	9.078	6.829	11.653	30.10	
$BaGe_2$-tri	Cal	4.344	4.344	5.435	29.59	38.60
$BaGe_2$-cub	Cal	7.088	7.088	7.088	29.68	38.31
$BaGe_2$-tet	Cal	4.882	4.882	15.031	29.86	35.64
	Exp [23]	4.769	4.769	14.737		
$SrGe_2$-ort	Cal	9.058	6.674	11.351	28.61	29.12
	Exp [17]	8.739	6.567	11.215	26.82	
$SrGe_2$-tri	Cal	4.204	4.204	5.256	26.83	41.50
	Exp [18]	4.104	4.104	5.165	25.11	
$SrGe_2$-cub	Cal	6.887	6.887	6.887	27.23	41.62
$SrGe_2$-tet	Cal	4.693	4.693	14.716	27.01	39.78

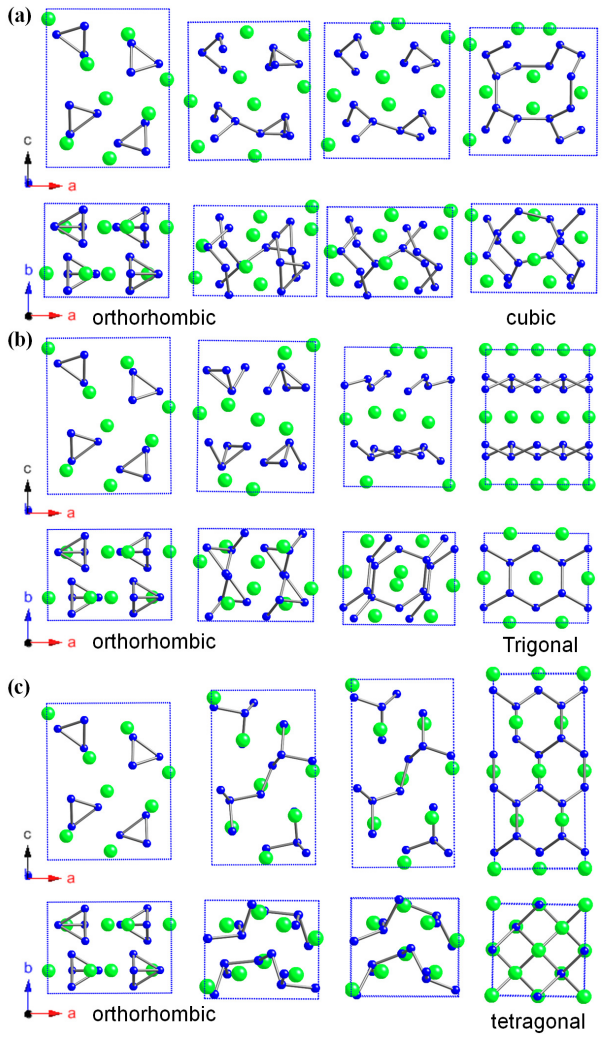

FIG. 2: (color online) Top and side views of the structures along the pathways to form cubic, trigonal and tetragonal $BaSi_2$ starting from the orthorhombic phase at 4 GPa. (a) Conversion process orthorhombic → cubic with bond breaking along the b[010] direction. The intermediate structures along the pathway are in $P2_1$ (No. 4) monoclinic symmetry. (b) Conversion process orthorhombic → trigonal with the shortening in the a_{ort} and c_{ort} direction and elongation in the b_{ort} direction. The intermediate structures along the pathway are in $P2_1/C$ (No. 14) monoclinic symmetry. (c) Conversion process orthorhombic → tetragonal with the shortening in the a_{ort} direction and elongation in the c_{ort} direction. The intermediate structures along the pathway are in $P2_12_12_1$ (No. 19) orthorhombic symmetry. The small (blue) and large (green) circles denote (Si,Ge) and (Ba,Sr) atoms, respectively.

$ThSi_2$-type tetragonal, and $EuGe_2$-type trigonal phases under pressure. For the transformation of the orthorhombic $BaSi_2$ to the cubic $BaSi_2$ phase [see Fig. 2(a)], b_{ort} = 6.827 Å → a_{cub} = 6.820 Å, c_{ort} = 11.716 Å → $\sqrt{2}a_{cub}$ = 9.645 Å, and a_{ort} = 9.224 Å → $\sqrt{2}a_{cub}$ = 9.645 Å, with about -18% shortening in the c_{ort} direction and about +4.6% elongation in the a_{ort} direction. Meanwhile, four Si_4 tetrahedra convert to four fourfold helices with bond breaking along the b[010] direction and rebonding with torsion angles of 60^o between the helical chains to form the 3D3C cubic net [34]. Throughout this pathway, the intermediate structures are all in $P2_1$ (No. 4) monoclinic symmetry, and the ∠Si-Si-Si bond angle changes from 60^o in Si_4 tetrahedra to 118^o in fourfold helices. As a result, one orthorhombic unit-cell is converted into two cubic unit-cells with 4 fourfold helices. For the transformation of the orthorhombic $BaSi_2$ into the trigonal $BaSi_2$ phase [see Fig. 2(b)], a_{ort} = 9.224 Å → $2a_{tri}$ = 8.204Å, b_{ort} = 6.827 Å → $\sqrt{3}a_{tri}$ = 7.105 Å, and c_{ort} = 11.716 Å → $2c_{tri}$ = 10.890 Å, with about -7% shortening in c_{ort}, -11% shortening in a_{ort} and +4% elongation in the b_{ort} direction. Along this pathway, four Si_4 tetrahedra convert to four distorted chains (parallel to the b[010] direction) with the bond breaking perpendicular to the c[001] axis, and then four chains rebond to each other to form corrugated Si layers with distorted six-membered rings. Throughout this pathway, the intermediate structures are all in $P2_1/C$ (No. 14) monoclinic symmetry, and the ∠Si-Si-Si bond angle changes from 60^o to 111.6^o. As a result, one orthorhombic unit-cell turns into four hexagonal cells. On the other hand, for the transformation of the orthorhombic $BaSi_2$ into the tetragonal $BaSi_2$ phase [see Fig. 2(c)], b_{ort} = 6.827 Å → $\sqrt{2}a_{tet}$ = 6.698 Å, a_{ort} = 9.224 Å → $\sqrt{2}a_{tet}$ = 6.698 Å, and c_{ort} = 11.716 Å → c_{tet} = 14.287 Å, with about -27% shortening in the a_{ort} direction and about +22% elongation in the c_{ort} direction. Along the pathway, four Si_4 tetrahedra convert to four flat Si_4 groups with bond breaking around the c[001] axis, and then the four flat Si_4 groups rebond to each other to form a 3D3C tetragonal net [see Fig. 2(c)]. Throughout this pathway, the intermediate structures are all in $P2_12_12_1$ (No. 19) orthorhombic symmetry, and the ∠Si-Si-Si bond angle changes from 60^o to 120^o. As a result, one orthorhombic unit-cell is converted into two tetragonal unit-cells.

Figure 3(a) shows the enthalpy along the pathways starting from orthorhombic $BaSi_2$ toward the formation of the cubic, tetragonal, and trigonal $BaSi_2$ phase at 4 GPa. The enthalpy increases initially due to the bond twisting and breaking of the Si_4 tetrahedra in the orthorhombic phase, and then it decreases with the relinking of Si-Si bonds. The conversion barriers are estimated to be 0.424 eV for orthorhombic → cubic, 0.430 eV for orthorhombic → trigonal, and 0.434 eV for orthorhombic → tetragonal. These results suggest the strong competing nature to form the cubic, trigonal and tetragonal structures. Among these reactions, however, the pathway toward the trigonal phase has the lowest enthalpy up to step 8 as shown in Fig. 3(a). Thus the orthorhombic-to-trigonal transition is more favored than the orthorhombic-to-cubic transition dynamically. Similar competing nature is also found in the hypothetical conversion of orthorhombic $SrSi_2$ toward cubic, trigonal

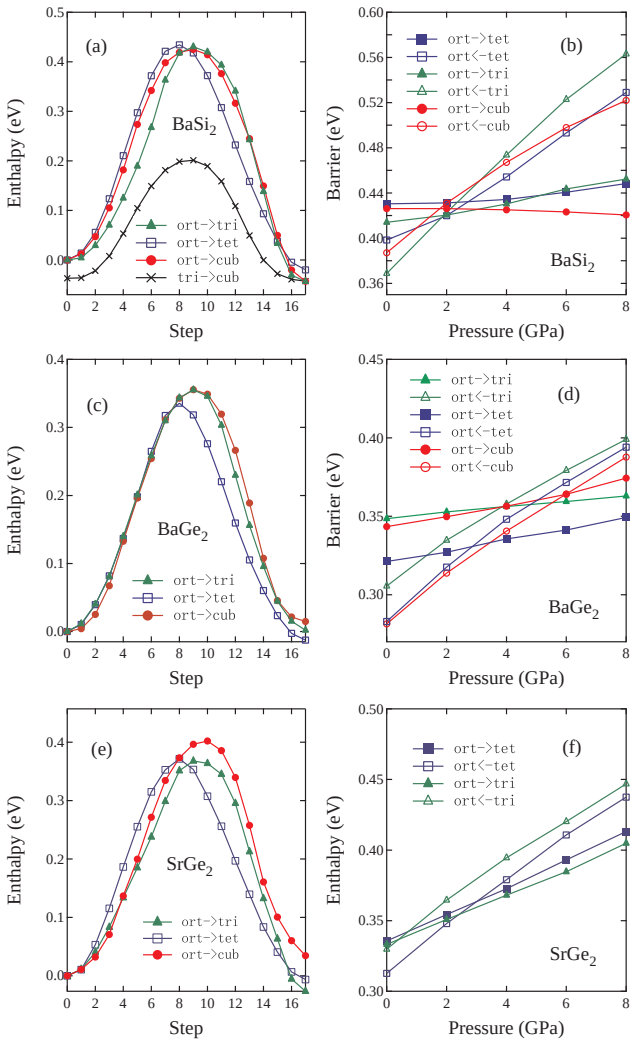

FIG. 3: (color online) (a,c,e) Enthalpy versus transformation pathways orthorhombic → cubic, trigonal, or tetragonal at 4 GPa for $BaSi_2$, $BaGe_2$, and $SrGe_2$, respectively. (b,d,f) Enthalpy barriers versus pressure for orthorhombic → cubic, tetragonal, and trigonal, respectively.

and tetragonal $SrSi_2$ [see Supplemental Material [35], Fig. S1]. On the other hand, the orthorhombic-to-cubic conversion is more favored energetically at low pressure and the orthorhombic-to-trigonal conversion is more favored energetically under high pressure [see Fig. 1(b)]. Experimentally, a two-stage reaction process of orthorhombic → trigonal → cubic is shown at 5.2 GPa up to 1133 K [19]. To clarify this point, we have also examined the second stage trigonal-to-cubic conversion process [see Supplemental Material [35], Fig. S2] and the corresponding enthalpy is plotted in Fig. 3(a). The conversion barrier is estimated to 0.24 eV at 4 GPa, which is smaller than 0.43 eV for the first stage orthorhombic-to-trigonal conversion. Consequently, cubic $BaSi_2$ can be easily synthesized by a two-stage reaction process.

We plot in Fig. 3(b) the enthalpy barriers versus pressure. With increasing pressure from 0 to 8 GPa, the barriers undergo only small changes from 0.429 to 0.421 eV for orthorhombic → cubic, 0.411 to 0.452 eV for orthorhombic → trigonal, and 0.430 to 0.448 eV for orthorhombic → tetragonal. These results show that pressure has little effect on the conversion barrier, which means these phase conversions require high temperature to overcome the large energy barriers. This is similar to the situation of phase conversion of graphite to diamond [36].

Experimentally, it has been reported that both the cubic and trigonal phases of $BaSi_2$ can be quenched to the ambient conditions [19, 20]. To clarify this point, the counterreaction barriers are also plotted in Fig. 3(b). With decreasing pressure from 8 to 0 GPa, the barriers decrease from 0.522 to 0.387 eV for cubic → orthorhombic, 0.523 to 0.362 eV for trigonal → orthorhombic, and 0.529 to 0.398 eV for tetragonal → orthorhombic. These results suggest that pressure has a considerable effect on lowering the kinetic barrier upon decompression. However, the counterreaction barriers remain at high values (∼ 0.39 eV at 0 GPa) that are comparable to the barriers encountered during the compression process (∼ 0.43 eV). As a result, the cubic and trigonal phases can be recovered and stabilized at ambient conditions due to a combination of the large counterreaction barriers (∼ 0.39 eV) and small energy differences (∼ 0.05 eV per atom) [see Fig. 1(b)].

For $BaGe_2$, as shown in Fig. 3(c,d), the orthorhombic → tetragonal conversion is clearly favorable by both kinetics and energetics. On the other hand, for $SrGe_2$ compound, the cubic structure is unfavorable in enthalpy as shown in Fig. 1(f) in a wide pressure range of 0∼10 GPa. There is a strong competing conversion pathway under pressure to form the trigonal or tetragonal structure [see Fig. 3(e,f)]; however, the orthorhombic → trigonal conversion is more favorable dynamically, similar to the case for $BaSi_2$ shown above.

It is noted that all of the Si and Ge sublattices satisfy the (8-N) rule that requires a formal transfer of valence electrons of the divalent metal atoms to Si or Ge atoms [22], which then become isoelectronic with group V elements. One can regard $BaSi_2$ formally as $Ba^{2+}[Si^-]_2$. The Si_4 tetrahedra in the orthorhombic phase resemble the structural arrangement of white phosphorus [37]; the corrugated layers of Si in the trigonal phase are similar to the crystal structures adopted by black phosphorus at high pressures [38]; and the cubic Si nets are congruent to the structure of cubic gauche nitrogen (cg-N) [39]. Here the divalent metals play a key role in stabilizing the three-connected net structures.

In summary, our *ab initio* calculations have revealed the phase stability and transformation mechanisms for several $BaSi_2$-type semiconductors. The results show that the tetrahedra in orthorhombic $BaSi_2$ and $SrGe_2$

tend to convert to corrugated layers dynamically under high pressure with bond breaking along the b[010] axis, and the Si-corrugated layers in trigonal $BaSi_2$ can further convert to cubic Si-net under low pressure driven by energetics. Moreover, Ge-tetrahedra in $BaGe_2$ tend to form a tetragonal-net structure with bond breaking around the c[001] axis. The large counterreaction barriers (∼0.39 eV) are comparable to that for the compression process reaction barriers (∼0.43 eV) for $BaSi_2$, which explains the high stability of the metallic metastable phases at the ambient conditions. Our results provide a comprehensive understanding of the experimental findings by unveiling the underlying energetic and kinetic mechanisms, which may shed light on other disilicides and digermanides.

This study was supported by the National Natural Science Foundation of China (Grant No. 11274356) and the Strategic Priority Research Program of the Chinese Academy of Sciences (Grant No. XDB07000000). C.F.C. acknowledges support by DOE under Cooperative Agreement DE-NA0001982. Y.K. acknowledges support by the CREST project headed by Professor M. Kotani and the Russian Megagrant Project No. 14.B25.31.0030. We are thankful to the crew of the Center for Computational Materials Science at IMR, Tohoku University for their support at the SR16000 supercomputing facilities.

* e-mail address:wjt@aphy.iphy.ac.cn

[1] J. Evers and A. Weiss, Mater. Res. Bull. **9,** 549 (1974).
[2] T. Nakamura, T. Suemasu, K. Takakura, F. Hasegawa, A. Wakahara, and M. Imai, Appl. Phys. Lett. **81,** 1032 (2002).
[3] S. Kishino, T. Imai, T. Iida, Y. Nakaishi, M. Shinada, Y. Takanashi, and N. Hamada, J. Alloys Compd. **428,** 22 (2007).
[4] Y. Matsumoto, D. Tsukada, R. Sasaki, M. Takeishi, and T. Suemasu, Appl. Phys. Express **2,** 021101 (2009).
[5] M. Imai, Phys. Status Solidi C **10,** 1728 (2013).
[6] T. Suemasu, K. Morita, and M. Kobayashi, J. Cryst. Growth **301-302,** 680 (2007).
[7] M. Kobayashi, Y. Matsumoto, Y. Ichikawa, D. Tsukada, and T. Suemasu, Appl. Phys. Express **1,** 051403 (2008).
[8] M. A. Khan, T. Saito, K. Nakamura, M. Baba, W. Du, K. Toh, K. Toko, and T. Suemasu, Thin Solid Films **522,** 95 (2012).
[9] W. J. Du, M. Suzuno, M. Ajmal Khan, K. Toh, M. Baba, K. Nakamura, K. Toko, N. Usami, and T Suemasu, Appl. Phys. Lett. **100,** 152114 (2012).
[10] M. Ajmal Khan, K. O. Hara, W. Du, M. Baba, K. Nakamura, M. Suzuno, K. Toko, N. Usami, and T. Suemasu, Appl. Phys. Lett. **102,** 112107 (2013).
[11] S. Koike, K. Toh, M. Baba, K. Toko, K. O. Hara, N. Usami, N.Saito, N. Yoshizawa, and T. Suemasu, J. Crystal Growth **378,** 198 (2013).
[12] H. K. Janzon, H. Schäfer, and A. Weiss, Z. Anorg. Allg. Chem. **372,** 87 (1970).
[13] H. Schäfer, K. H. Janzon, and A. Weiss, Angew. Chem. Int. Ed. Engl. **2,** 393 (1963).
[14] J. Evers, G. Oehlinger, and A. Weiss, Angew. Chem. Int. Ed. Engl. **17,** 538 (1978).
[15] J. Evers, G. Oehlinger, and A. Weiss, Angew. Chem. Int. Ed. Engl. **16,** 659 (1977).
[16] M. Pani and A. Palenzona, J. Alloys Compd. **462,** L9 (2008).
[17] A. Palenzona and M. Pani, J. Alloys Compd. **402,** 136 (2005).
[18] J. Evers, G. Oehlinger, and A. Weiss, Z. Naturforsch. B **32,** 1352 (1977).
[19] M. Imai, T. Hirano, T. Kikegawa, and O. Shimomura, Phys. Rev. B **55,** 132 (1997); *ibid.* **58,** 11 922 (1999).
[20] J. Evers, J. Solid State Chem. **32,** 77 (1980).
[21] J. Evers, J. Solid State Chem. **24,** 199 (1978); J. Phys. Chm. Solid **40,** 951 (1979).
[22] J. T. Vaughey, G. J. Miller, S. Gravelle, E. A. Leon-Escamilla, and J. D. Corbett, J. Solid State Chem. **133,** 501 (1997).
[23] J. Evers, G. Oehlinger, and A. Weiss, Z. Naturforsch. B **35,** 397 (1980).
[24] A. Palenzona and M. Pani, The phase diagram of the SrCGe system J. Alloys Compd. **402,** 136 (2005).
[25] K. Hashimoto, K. Kurosaki, Y. Imamura, H. Muta, and S. Yamanaka, J. Appl. Phys. **102,** 063703 (2007).
[26] D. B. Migas, V. L. Shaposhnikov, and V. E. Borisenko, Phys. Stat. Sol. **244,** 2611 (2007).
[27] M. Kumar, N. Umezawa, and M. Imai, J. Appl. Phys. **115,** 203718 (2014).
[28] J. T. Wang, C. F. Chen, H. Mizuseki, and Y. Kawazoe, Phys. Rev. Lett. **110,** 165503 (2013).
[29] G. Kresse and J. Furthmüller, Phys. Rev. B **54**, 11169 (1996); G. Kresse and J. Hafner, *ibid.* **47**, 558 (1993).
[30] Y. K. Zhang and W. T. Yang, Phys. Rev. Lett. **80,** 890 (1998).
[31] P. E. Blöchl, Phys. Rev. B **50**, 17953 (1994); G. Kresse and D. Joubert, Phys. Rev. B **59**, 1758 (1999).
[32] J. T. Wang, C. F. Chen, and Y. Kawazoe, Phys. Rev. Lett. **106,** 075501 (2011).
[33] M. Imai and T. Kikegawa, Chem. Mater. **15,** 2543 (2003).
[34] J. T. Wang, C. F. Chen, and Y. Kawazoe, Sci. Rep. **3,** 03077 (2013)
[35] See Supplemental Material at http://link.aps.org/ supplemental for the hypothetical orthorhombic $SrSi_2$ (Fig. S1) and the conversion pathway between trigonal and cubic $BaSi_2$ (Fig. S2).
[36] J. T. Wang, C. F. Chen, and Y. Kawazoe, Phys. Rev. B **84,** 012102 (2011).
[37] A. Simon, H. Borrmann, and H. Craubner, Phosphorus and Sulfur and the Related Elements, **30,** 507 (1987); H. Okudera, R. E. Dinnebier, and A. Simon, Z. Kristallogr. **220,** 259 (2005).
[38] J. C. Jamieson, Science **139,** 1291 (1963).
[39] M. I. Eremets, A. G. Gavriliuk, I. A. Trojan, D. A. Dzivenko, and R. Boehler, Nature Mater. **3,** 558 (2004).